Heat and mass transfer analysis in unsteady boundary layer flow of Maxwell nanofluid over a stretching sheet

Eshetu Haile[1,*], Bandari Shankar[2], Eleni Seid[3] and Raja Shekar[4]

[1]Department of Mathematics, Bahir Dar University, Bahir Dar, Ethiopia
[2]Department of Mathematics, CVR College of Engineering, Hyderabad, India
[3]Department of Mathematics, Debre Tabor University, Debre Tabor, Ethiopia
[4]Department of Mathematics, JNTU College of Engineering, Hyderabad, India

ABSTRACT

This paper presents analytic study of heat and mass transfer in a two-dimensional, unsteady flow of Maxwell nanofluids over a horizontal stretching sheet. The non-linear governing equations with the relevant boundary conditions have been simplified by using similarity transformations and the resulting equations are solved by using the homotopy analysis method. The convergence and accuracy of the solutions are verified. Impacts of magnetic field, thermal radiation, heat source, surface permeability and chemical reaction on velocity, temperature and nanoparticles volume fraction profiles are examined and presented in graphical and tabular forms. The study reveals that increasing the effect of heat source maximizes the temperature profile whereas it reduces the nanoparticle volume fraction profile in the boundary layer. On the other hand, the increase in chemical reaction is found to enhance the nanoparticle concentration.

Keywords: Homotopy Analysis Method; Unsteady Flow; Boundary Layer Flow; Maxwell Nanofluid
DOI: https://dx.doi.org/10.4314/ejst.v13i2.1

INTRODUCTION

Due to the complex nature of non-Newtonian fluids in response to the applied stress tensor, various mathematical models have been proposed by researchers to examine and predict the flow characteristics of such fluids. For instance, when the applied shear stress is removed from the so-called *viscoelastic fluids*, the rate of deformation gradually decreases. This phenomenon is known as the *stress relaxation*. Moreover, the time taken by the fluid to recover upon the

* Corresponding author: eshetuhg@gmail.com

elimination of the applied stress is called *relaxation time*. Maxwell model, proposed in 1867 by J.C. Maxwell, is one of the viscoelastic models used to examine the shear thinning characteristics of many industrially important fluids such as paints, paper pulps, shampoos and liquid polymers.

The embedding of nanoparticles in the conventional heat transferring liquids improves thermal conductivity of the fluids (Choi and Eastman, 1995). In view of the practical applications of Maxwell nanofluids, several researchers have reported their study on the influences of various thermo-physical parameters in the boundary layer flow of such fluids over horizontally stretching surfaces. For instance, Nadeem *et al*. (2013) shows that the Brownian motion parameter reduces the rate of heat transfer but enhances the rate of mass transfer. Ramesh and Gireesha (2014) reported a numerical investigation of the heat source/sink effects. It was found that the local Nusselt number is smaller and local Sherwood number is higher for Maxwell fluids compared to Newtonian fluids. Awais *et al*. (2015) investigated the heat generation/absorption effects by using both the analytic and numerical methods. They pointed out that the increase in the Deborah number slows down velocity of the fluid. Moreover, the temperature of the fluid flow system was enhanced and diminished by the presence of the heat source and the heat sink, respectively.

Recently, Elbashbeshy *et al*. (2018) investigated heat and mass transfer of the flow of a Maxwell nanofluid over a stretching surface with variable thickness embedded in a porous medium by using the Rung-Kutta fourth/fifth order method coupled with shooting technique. The effects of chemical reaction and heat source/sink on a steady magnetohydrodynamic mixed convective boundary layer flow of a Maxwell nanofluid over a porous exponentially stretching sheet was studied by Sravanthi and Gorla (2018). Further, Ijaz and Ayub (2019) considered nonlinear convective flow of Maxwell nanofluid over inclined stretched cylinder.

On the other hand, some studies considered the effect of unsteadiness parameter in their boundary layer flow analysis. For instance, the researchers Mukhopadhyay and Bhattacharyya (2012) employed the shooting method to analyze the unsteady flow of Maxwell fluid in the presence of first order chemical reaction. The study showed that velocity of the fluid initially decreases while nanoparticles volume fraction profile decreases significantly due to the increase in the unsteadiness parameter. Also increasing values of the Maxwell parameter was found to retard velocity of the fluid but it enhanced the nanoparticles volume fraction profile. Mabood *et al*. (2016) applied the implicit finite difference method with quasi-linearization technique to examine unsteady flow of Maxwell fluid over a stretching surface in the presence of uniform magnetic field, nonlinear thermal radiation and first-order chemical reaction

with convective boundary conditions. This study revealed that for larger Maxwell parameter, the viscous forces are dominant enough to restrict the fluid motion. Significant effects of thermal and nanoparticles volume fraction Biot numbers were observed in influencing the temperature and nanoparticles volume fraction profiles, respectively.

The purpose of this study was to examine the influences of pertinent parameters such as magnetic field, thermal radiation, heat source, surface permeability and chemical reaction on velocity, temperature and nanoparticles volume fraction profiles in the boundary layer flow region. Moreover, the study employs the homotopy analysis method and the results were then compared with that of some previously published works.

MATHEMATICAL FORMULATIONS

In the present study, unsteady laminar flow of an incompressible electrically conducting Maxwell nanofluid over a heated and permeable horizontal sheet is considered. A non-uniform transversal magnetic field of strength $B = \frac{B_0}{\sqrt{1-at}}$, where B_0 is the initial magnetic field strength, is applied normal to the surface as shown in Figure 1. The flow above the x-axis (y >0) induced by the motion of a horizontal sheet emerging from a slit and moving with a non-uniform velocity of $U_w(x,t) = \frac{cx}{1-at}$ is considered.

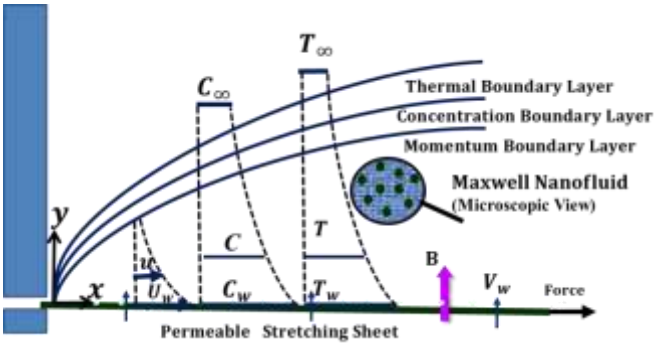

Figure 1. Sketch of the flow problem

Using the Cartesian coordinate system with origin at the slit and applying the Rosseland diffusion and the boundary layer approximations, we re-wrote the flow problem of Madhu *et al*. (2017) as follows:

$$\frac{\partial u}{\partial x}+\frac{\partial v}{\partial y}=0 \tag{1}$$

$$\frac{\partial u}{\partial t}+u\frac{\partial u}{\partial x}+v\frac{\partial u}{\partial y}=\upsilon\frac{\partial^2 u}{\partial y^2}-\lambda_0\left(u^2\frac{\partial^2 u}{\partial x^2}+v^2\frac{\partial^2 u}{\partial y^2}+2uv\frac{\partial^2 u}{\partial x\partial y}\right)-\frac{\sigma {B_0}^2}{\rho f}u, \tag{2}$$

$$\frac{\partial T}{\partial t}+u\frac{\partial T}{\partial x}+v\frac{\partial T}{\partial y}=\alpha\frac{\partial^2 T}{\partial y^2}+\tau\left[D_B\frac{\partial C}{\partial y}\frac{\partial T}{\partial y}+\frac{D_T}{T_\infty}\left(\frac{\partial T}{\partial Y}\right)^2\right]+\frac{16\sigma^* {T_\infty}^3}{3(\rho c_p)_f k^*}\frac{\partial^2 T}{\partial y^2}+\frac{Q_0}{(\rho C_p)_f}(T-T_\infty), \tag{3}$$

$$\frac{\partial C}{\partial t}+u\frac{\partial C}{\partial x}+v\frac{\partial C}{\partial y}=D_B\frac{\partial^2 C}{\partial y^2}+\frac{D_T}{T_\infty}\frac{\partial^2 T}{\partial y^2}-K_r(C-C_\infty)\,, \tag{4}$$

where t is the time variable, $(u,\ v)$ are the velocity components in the x and y-directions; ρ_f and λ_0 denote density and viscoelasticity of the nanofluid, respectively; $\upsilon=\frac{\mu}{\rho_f}$ is kinematicviscosity with μ representing coefficient of dynamic viscosity; T and C denote temperature and nanoparticles volume fraction; T_∞ and C_∞ are the corresponding ambient values of temperature and nanoparticle volume fraction; $\alpha=\frac{k}{(\rho C_p)_f}$ is thermal diffusivity and $\tau=\frac{(\rho C_p)_p}{(\rho C_p)_f}$ is ratio of effective heat capacities of nanoparticle and the ordinary fluid; D_B and D_T are the Brownian and thermophoresis diffusion coefficients, respectively; k^* and σ^* are the mean absorption and the Stefan-Boltzmann constants, respectively; the coefficient Q_0 stands for heat source and K_r denotes the chemical reaction rate. We consider the following boundary conditions:

At $y=0$,

$$\boldsymbol{u=U_w(x,t)=\frac{cx}{1-at}, v=V_w(x,t)=\frac{-v_0}{\sqrt{1-at}}, T=T_w(x,t)=T_\infty+\frac{cx}{(1-at)^2}, D_B\frac{\partial C}{\partial y}+\frac{D_T}{T_\infty}\frac{\partial T}{\partial y}=0}, \tag{5}$$

and as $y\to\infty$, we have

$$u\to 0,\qquad T\to T_\infty\,, C\to C_\infty \tag{6}$$

where U_w and T_w are velocity and temperature of the surface, respectively; V_w is the mass transmission at the surface of the stretching sheet; v_0 is the constant value of velocity; a and c are positive constants denoting velocity rate of the stretching sheet and the fluid, respectively.

Next, we introduce the following similarity transformations:

$$\boldsymbol{\eta=y\sqrt{\frac{c}{\nu(1-at)}},\quad \psi=\sqrt{\frac{c\nu}{1-at}}xf(\eta), T=T_\infty+\frac{cx}{(1-at)^2}\theta(\eta),\quad C=C_\infty+\frac{cx}{(1-at)^2}\varphi(\eta)} \tag{7}$$

where η stands for the dimensionless similarity variable; $f(\eta)$, $\theta(\eta)$ and $\varphi(\eta)$ denote the dimensionless functions for velocity, temperature and nanoparticles volume fraction, respectively.

Using the stream function $\psi(x,y)$ having the property $u = \frac{\partial \psi}{\partial y}$ and $v = -\frac{\partial \psi}{\partial x}$, the continuity equation for velocity in Equation (1) is identically satisfied. Computing the required partial derivatives with respect to η and substituting the values into the governing equations (2-4), the following system of ordinary differential equations are obtained:

$$f''' - A\left(\frac{\eta}{2}f'' + f'\right) - f'^2 + ff'' - \lambda(f^2 f''' - 2ff'f'') - Mf' = 0, \quad (8)$$

$$\frac{1}{Pr}\left(1 + \frac{4Rd}{3}\right)\theta'' - \frac{A}{2}(\eta\theta' + 4\theta) - f'\theta + f\theta' + N_b\theta'\varphi' + N_t\theta'^2 + Q\theta = 0, \quad (9)$$

$$\varphi'' + \frac{N_t}{N_b}\theta'' - s_c\left(\frac{A}{2}(\eta\varphi' + 4\varphi) + f'\varphi - f\varphi' - \gamma\varphi\right) = 0, \quad (10)$$

where the prime ' indicates differentiation with respect to η; $A = \frac{a}{c}$ is the unsteadiness parameter; $M = \frac{\sigma {B_0}^2}{a\rho f}$ denotes the external magnetic field parameter; $\lambda = \frac{c\lambda_0}{1-at}$ is the Deborah number representing the Maxwell viscoelastic parameter; $P_r = \frac{v}{\alpha}$ and $S_c = \frac{v}{D_B}$ are the Prandtl number and the Schmidt number, respectively; $R_d = \frac{4\sigma^* {T_\infty}^3}{kk^*}$ is thermal radiation parameter; $N_b = \frac{\tau D_B(C_w - C_\infty)}{v}$ and $N_t = \frac{\tau D_T(T_w - T_\infty)}{vT_\infty}$ are the Brownian motion and thermophoresis parameters, respectively; $Q = \frac{xQ_0}{(\rho C_p)_f U_w}$ is the heat source parameter and $\gamma = \frac{K_r x}{U_w}$ is chemical reaction parameter. Also employing the similarity transformation in Equation (5), the boundary conditions can be reduced as follows:

$$f(0) = S,\ f'(0) = 1, \theta(0) = 1,\ N_b\varphi'(0) + N_t\theta'(0) = 0\,, \quad (11)$$

and as $\eta \to \infty$,

$$f'(\eta) \to 0, \qquad \theta(\eta) \to 0, \qquad \varphi(\eta) \to 0 \quad (12)$$

where the parameter $S = \frac{v_0}{\sqrt{cx}}$ is the transpiration parameter of the wall.

From practical point of view, it is also useful to predict the behavior of Skin friction C_f, local Nusselt number Nu_x and Sherwood number Sh_x in the boundary layer region are given by

$$Re_x{}^{1/2}C_f = 2(1+\lambda)f''(0), \qquad Re_x{}^{-1/2}Nu_x = -\left(1 + \frac{4Rd}{3}\right)\theta'(0), \qquad Re_x{}^{-\frac{1}{2}}Sh_x = -\varphi'(0), \quad (13)$$

where $\mathrm{Re}_x = \frac{xU_w}{v}$ is the local Reynolds number.

METHOD OF SOLUTION

The homotopy analysis method (HAM), first proposed in 1992 by Liao, has been one of the most efficient analytic methods that is known to give convenient mechanism of ensuring the convergence of its solutions. In this study, the method can be implemented by following the following major procedures; details of the method can be referred in Liao (2003).

Based on the equations (8)-(10), the non-linear operators can be defined as:

$$N_f = \frac{\partial^3 \emptyset_f}{\partial \eta^3} - A\left(\frac{\eta}{2}\frac{\partial^2 \emptyset_f}{\partial \eta^2} + \frac{\partial \emptyset_f}{\partial \eta}\right) - \left(\frac{\partial \emptyset_f}{\partial \eta}\right)^2 + \emptyset_f \frac{\partial^2 \emptyset_f}{\partial \eta^2} - \lambda\left(\emptyset_f{}^2 \frac{\partial^3 \emptyset_f}{\partial \eta^3} - 2\emptyset_f \frac{\partial \emptyset_f}{\partial \eta}\frac{\partial^2 \emptyset_f}{\partial \eta^2}\right) - M\frac{\partial \emptyset_f}{\partial \eta} \quad (14)$$

$$N_\theta = \left(1 + \frac{4Rd}{3}\right)\frac{\partial^2 \emptyset_\theta}{\partial \eta^2} - \frac{A}{2}\left(\eta\frac{\partial \emptyset_\theta}{\partial \eta} + 4\emptyset_\theta\right) - \frac{\partial \emptyset_f}{\partial \eta}\emptyset_\theta + \emptyset_f\frac{\partial \emptyset_\theta}{\partial \eta} + Nb\frac{\partial \emptyset_\theta}{\partial \eta}\frac{\partial \emptyset_\varphi}{\partial \eta} + Nt\left(\frac{\partial \emptyset_\theta}{\partial \eta}\right)^2 + Q\emptyset_\theta \quad (15)$$

$$N_\varphi = \frac{\partial^2 \emptyset_\varphi}{\partial \eta^2} - Sc\left[\frac{A}{2}\left(\eta\frac{\partial \emptyset_\varphi}{\partial \eta} + 4\emptyset_\varphi\right) + \frac{\partial \emptyset_f}{\partial \eta}\emptyset_\varphi - \emptyset_f\frac{\partial \emptyset_\varphi}{\partial \eta} - \gamma\emptyset_\varphi\right] + \frac{Nt}{Nb}\frac{\partial^2 \emptyset_\theta}{\partial \eta^2}, \quad (16)$$

where $\emptyset_f$, $\emptyset_\theta$ and $\emptyset_\varphi$ are the homotopy approximations of f, θ and φ, respectively satisfying the initial and boundary conditions.

According to Liao (2003), the corresponding zeroth-order deformation equations can be constructed as

$$(1-q)\mathcal{L}_f[\emptyset_f - f_0] = q\hbar_f H_f N_f \quad (17)$$

$$(1-q)\mathcal{L}_\theta[\emptyset_\theta - \theta_0] = q\hbar_\theta H_\theta N_\theta \quad (18)$$

$$(1-q)\mathcal{L}_\varphi[\emptyset_\varphi - \varphi_0] = q\hbar_\varphi H_\varphi N_\varphi \quad (19)$$

where $q \in [0,1]$ is the embedding parameter; $\mathcal{L}_f$, $\mathcal{L}_\theta$ and $\mathcal{L}_\varphi$ are the auxiliary linear operators selected as:

$$\mathcal{L}_f(f) = \frac{d^3 f}{d\eta^3} - \frac{df}{d\eta}, \quad \mathcal{L}_\theta(\theta) = \frac{d^2\theta}{d\eta^2} + \frac{d\theta}{d\eta}, \quad \mathcal{L}_\varphi(\varphi) = \frac{d^2\varphi}{d\eta^2} + \frac{d\varphi}{d\eta} \quad (20)$$

Satisfying the properties

$$L_f[C_1 + C_2 e^{-\eta} + C_3 e^{\eta}] = 0, \quad L_\theta[C_4 + C_5 e^{-\eta}] = 0, \quad L_\varphi[C_6 + C_7 e^{-\eta}] = 0, \quad (21)$$

with $C_i (i = 1-7)$ are constants to be determined from the boundary conditions; f_0, θ_0 and φ_0 are the initial approximations given by

$$f_0(\eta) = 1 + s - e^{-\eta}, \qquad \theta_0(\eta) = e^{-\eta},\ \varphi_0(\eta) = -\frac{N_t}{N_b}e^{-\eta} \tag{22}$$

H_f, H_θ and H_φ are the auxiliary functions defined as:

$$H_f(\eta) = H_\theta(\eta) = H_\varphi(\eta) = e^{-\eta}, \tag{23}$$

where $\hbar_f$, $\hbar_\theta$ and $\hbar_\varphi$ are the convergence-control parameters to be determined later.

One can easily verify in Equations (17) to (19) that as the embedding parameter q increases from 0 to 1, the homotopy solutions $\emptyset_f$, $\emptyset_\theta$ and $\emptyset_\varphi$ vary continuously from the initial approximations f_0, θ_0 and φ_0 to the exact solutions $f(\eta)$, $\theta(\eta)$ and $\varphi(\eta)$.

Substituting the Maclaurin series expansion of $\emptyset_f, \emptyset_\theta$ and $\emptyset_\varphi$ into the zeroth-order deformation equations and equating the coefficients of like powers of q; or by differentiating the zeroth- order deformation equations m times with respect to q, then dividing the resulting equations by m! and finally setting $q = 0$, the following mth-order deformation equations are obtained:

$$\mathcal{L}_f[f_m(\eta) - \chi_m f_{m-1}(\eta)] = \hbar_f \mathrm{H}_f \mathcal{R}^f_{m-1}(\eta) \tag{24}$$
$$\mathcal{L}_\theta[\theta_m(\eta) - \chi_m \theta_{m-1}(\eta)] = \hbar_\theta \mathrm{H}_\theta \mathcal{R}^\theta_{m-1}(\eta) \tag{25}$$
$$\mathcal{L}_\varphi[\varphi_m(\eta) - \chi_m \varphi_{m-1}(\eta)] = \hbar_\varphi \mathrm{H}_\varphi \mathcal{R}^\varphi_{m-1}(\eta) \tag{26}$$

where $\chi_m = \begin{cases} 0, & \text{if m} \le 1 \\ 1, & \text{if m} > 1 \end{cases}$ is the unit step function and

$$\mathcal{R}^f_{m-1} = f'''_{m-1} - A\left(\frac{\eta}{2}f'''_{m-1} - f'_{m-1}\right) - \sum_{k=0}^{m-1} f_k{}' f'_{m-1-k} + \sum_{k=0}^{m-1} f_k f''_{m-1-k} - \lambda\left(\sum_{k=0}^{m-1}\sum_{r=0}^{k} f_{k-r} f_{m-r-1} f_m''' - 2\sum_{k=0}^{m-1}\sum_{r=0}^{k} f_{m-k-1} f'_{k-r} f_r''\right) - M f'_{m-1} \tag{27}$$

$$\mathcal{R}^\theta_{m-1} = \frac{1}{\mathrm{Pr}}\left(1 + \frac{4Rd}{3}\right)\theta''_{m-1} - \frac{A}{2}(\eta\theta'_{m-1} + 4\theta_{m-1}) - \sum_{k=0}^{m-1} \theta_k f'_{m-k-1} + \sum_{k=0}^{m-1} f_k \theta'_{m-k-1} + Nb\sum_{k=0}^{m-1} \theta'_{m-1} f'_{m-1-k} + Nt\sum_{k=0}^{m-1} f_k' f'_{m-1-k} + Q\theta_{m-1} \tag{28}$$

$$\mathcal{R}^{\varphi}_{m-1} = \varphi''_{m-1} - Sc\left[\frac{A}{2}\left(\eta\varphi'_{m-1} + 4\varphi_{m-1}\right) + \sum_{k=0}^{m-1} f'_{m-1-k}\,\varphi_k - \sum_{k=0}^{m-1} f_k\,\varphi'_{m-1-k} - \gamma\varphi_{m-1}\right] + \frac{Nt}{Nb}\theta''_{m-1} \quad (29)$$

where the primes denote differentiation with respect to η.

Taking the inverse of the linear operators on both sides of the higher order deformation equations, one can get the following iterative formula: $f_m(\eta) = \chi_m f_{m-1}(\eta) + \hbar_f \mathcal{L}_f^{-1}\left[H_f R^f_{m-1}(\eta)\right]$ (30)

$$\theta_m(\eta) = \chi_m \theta_{m-1}(\eta) + \hbar_\theta \mathcal{L}_\theta^{-1}\left[H_\theta R^\theta_{m-1}(\eta)\right] \quad (31)$$

$$\varphi_m(\eta) = \chi_m \varphi_{m-1}(\eta) + \hbar_\varphi \mathcal{L}_\varphi^{-1}\left[H_\varphi R^\varphi_{m-1}(\eta)\right] \quad (32)$$

To carry out the computation, the HAM-based Mathematica package BVPh 2.0 was adopted (Zhao and Liao, 2013). But to ensure the convergence of the HAM solutions, the graphs of the kth-partial sums of the functions against the convergence-control parameters were plotted as shown in Figure 2.

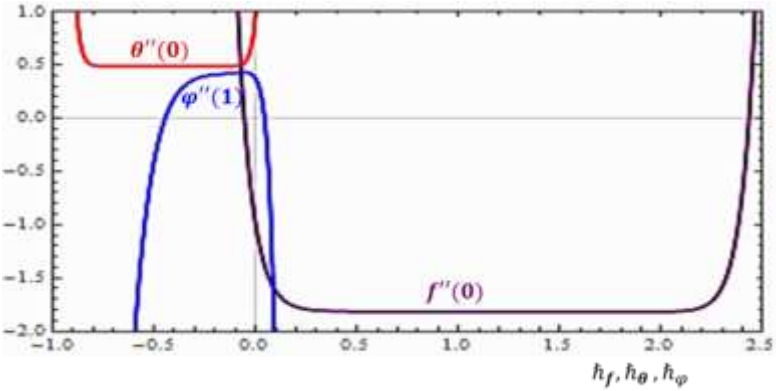

Figure 2. $\hbar$ − curves

Figure 2 indicates that the intervals $0.3 < \hbar_f < 2.1, -0.9 < \hbar_\theta < -0.1$ and $-0.3 < \hbar_\varphi < 0.0$ are the valid regions for the range of admissible values of the convergence-control parameters. According to Liao (2003), taking any value for the convergence-control parameters will make the HAM solution convergent. The convergence of the series solution can also be determined from examining the squared residual errors as presented in Table 1. It displays that

the values of the selected quantities of interest are convergent before the 30th order HAM. Also, as the order of HAM increases, the errors are getting smaller.

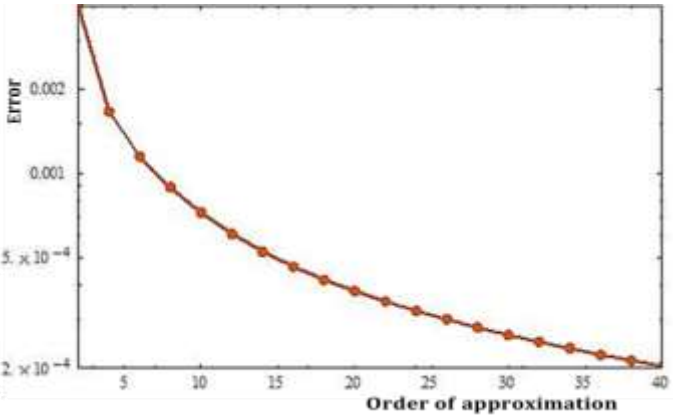

Figure 3. Total squared residual error for the 40th HAM approximation

It can be seen from the above figure that increasing the order of HAM approximation reduces the squared residual errors which ensures the validity of the method in the given flow problem.

Table 1. Convergence of HAM solution.

Order of HAM approximation	$-f''(0)$	$-\theta(0)$	$-\varphi(0)$	Squared residual errors		
				ε_f	ε_θ	ε_φ
2	1.9283	0.54716	1.26634	9.2×10^{-5}	2.6×10^{-3}	1.3×10^{-3}
6	1.81483	0.48619	1.36611	1.4×10^{-6}	8.2×10^{-4}	3.3×10^{-4}
10	1.81640	0.48531	1.37948	2.5×10^{-7}	5.2×10^{-4}	2.1×10^{-4}
14	1.81680	0.48529	1.38809	7.5×10^{-8}	3.7×10^{-4}	1.5×10^{-4}
18	1.81695	0.48529	1.39421	3.0×10^{-8}	3.0×10^{-4}	1.2×10^{-4}
22	1.81702	0.48529	1.39884	1.4×10^{-8}	2.5×10^{-4}	1.0×10^{-4}
26	1.81706	0.48529	1.40251	8.0×10^{-9}	2.1×10^{-4}	8.8×10^{-5}
30	1.81708	0.48529	1.40251	4.8×10^{-9}	1.9×10^{-5}	7.7×10^{-5}
34	1.81710	0.48529	1.40550	3.1×10^{-9}	1.7×10^{-5}	6.9×10^{-5}
38	1.81710	0.48528	1.40800	2.1×10^{-9}	1.5×10^{-5}	6.2×10^{-5}

To ensure the validity of our results again, we make comparisons with some previously published works in the absence of the extended physical effects as depicted in Table 2. The table justifies that the values of $f''(0)$ obtained in this study are in a nice agreement with the aforementioned published results.

Table 2. Comparisons of the present study with previously published works on the values of $f''(0)$ against some values of the unsteadiness parameter A when $\lambda = M = S = Q = \gamma = 0$

A	(Sharidan *et al*., 2006)	(Chamkha *et al*., 2010)	(Mukhopadhyay *et al*., 2013)	(Madhu *et al*., 2017)	Present Study
0.8	-1.261042	-1.261512	-1.261479	-1.26121	-1.261844
1.2	-1.377722	-1.378052	-1.377850	-1.37763	-1.377947

RESULTS AND DISCUSSION

In this section, we present the most significant results of our study in graphical and tabular forms followed by brief discussions. The parameter values $A = 0.1$, $\lambda = 0.2$, $M = 1$, $Pr = 0.5$, $R_d = 0.1$, $N_b = N_t = 0.2$, $S = 0.4$, $S_c = 1$, $Q = \gamma = 0.1$ and the optimal values for the convergence control parameters $\hbar_f \approx 1.4468$, $\hbar_\theta \approx -0.5941$ and $\hbar_\varphi \approx -0.1992$ have been used throughout this study unless and otherwise stated. The influences of various thermo-physical parameters on fluid velocity $f'(\eta)$, temperature $\theta(\eta)$ and nanoparticle volume fraction $\varphi(\eta)$ profiles in the boundary layer region are presented.

It can be seen from Figure 4 that all the velocity, temperature and nanoparticles volume fraction profiles are decreasing functions of the unsteadiness parameter A. It is observed that nanoparticles volume fraction and the temperature profiles decrease faster than velocity of the fluid in the boundary layer region. This is also evident from the fact that as the unsteadiness parameter increases, the velocity of the stretching sheet decreases which causes the transfer of less amount of heat and mass from the sheet to the boundary layer region.

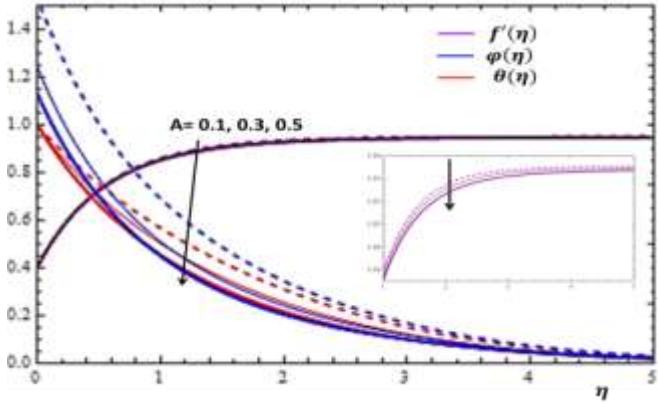

Figure 4. Effects of unsteadiness parameter A on velocity and temperature profiles.

The effects of the Maxwell viscoelastic parameter λ has been studied and presented in Figure 5. It can be observed that the temperature and nanoparticles volume fraction profiles can be enhanced by increasing the parameter λ. On the other hand, the velocity falls rapidly with increasing values of λ. Physically, this corresponds to the fact that as λ increases, the fluid is getting thicker.

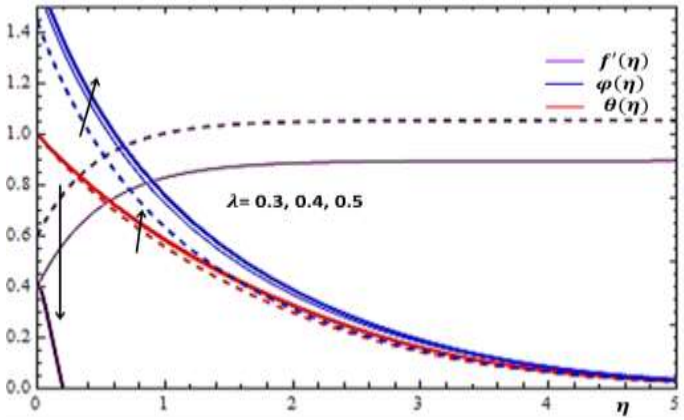

Figure 5. Impacts of λ on velocity, temperature and concentration profiles.

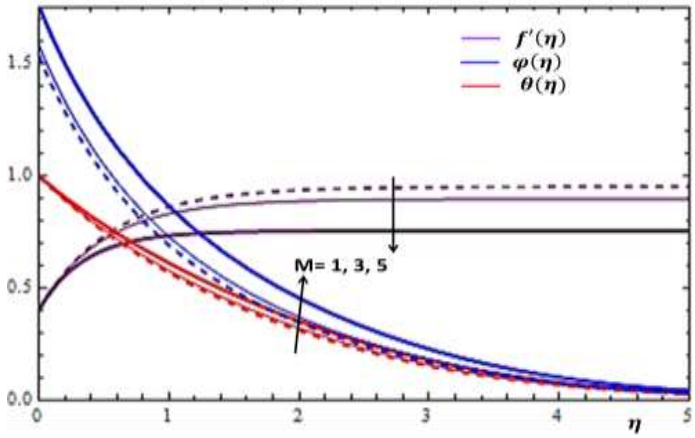

Figure 6. Effects of M on velocity, temperature and concentration profiles.

Impacts of the external magnetic field in the flow field has been studied and presented in Figure 6. The results in the figure display that the increase in external magnetic field slows down the fluid velocity but it enhances the

nanoparticles volume fraction and temperature profiles. This is true as the increase in magnetic field produces a resistive force, called the Lorentz force, which retards the motion of the fluid. On the other hand, this resistive force causes the increase in the temperature and nanoparticles volume fraction in the boundary layer. The effect of thermal radiation in the boundary layer region has been presented in Figure 7. The figure displays that the increase in thermal radiation causes the raise in temperature and the fall in concentration profiles. This is because higher thermal radiation causes the increase in the kinetic energy of the fluid molecules and higher heat flux near the stretching surface. It can also be noted that there is no significant variation of the velocity with the change in the parameter.

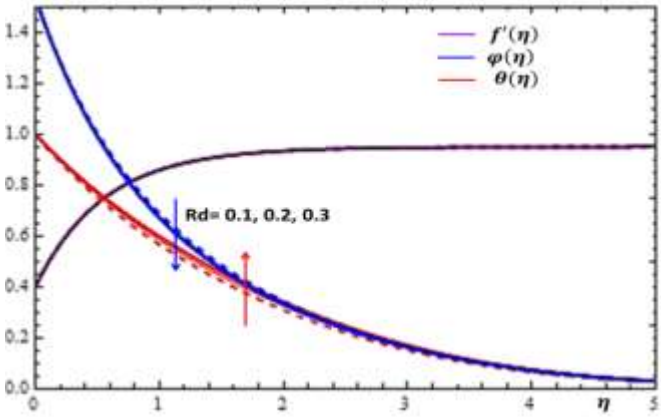

Figure 7. Impacts of R_d on velocity, temperature and concentration profiles

As pointed out in Figure 8, the increase in chemical reaction found to increase the concentration profile but it does not show any significant influence on the velocity and temperature profiles. The reason is that the increase in constructive chemical reaction has a tendency to enhance mass diffusion.

The heat source parameter Q has been used to describe the impacts of heat generation and heat absorption as shown in Figure 9.

According to the result in Figure 9, the increase in heat source parameter leads to the increase in the temperature and the decrease in concentration profiles. It can also be observed that velocity profile does not vary with the heat source parameter.

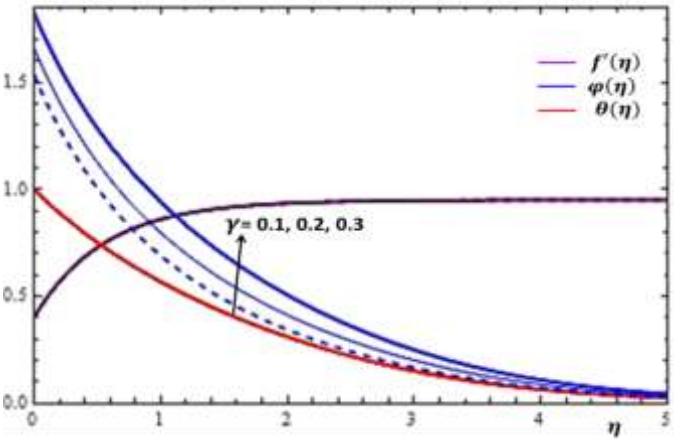

Figure 8. Effects ofγon velocity, temperature and concentration profiles.

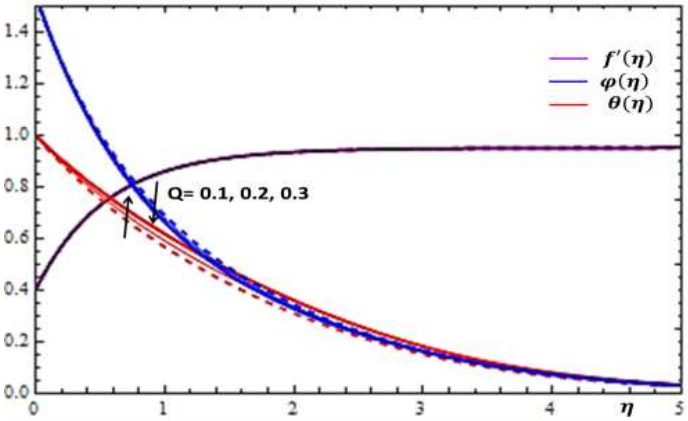

Figure 9. Effects of Q on velocity, temperature and concentration profiles.

The permeability effect of the stretching sheet has been examined and illustrated in Figure 10. It can be seen from Figure 10 that both the temperature and nanoparticles volume fraction profiles are decreasing while the velocity profile is increasing with the increase in the permeability parameter. The impacts of some pertinent parameters on local skin friction coefficient (C_f), Nusselt number (Nu_x) and Sherwood number (Sh_x) were examined and expressed in terms of the coefficients $f''(0), -\theta'(0)$and $-\varphi'(0)$, respectively.

The variations of skin friction coefficient for different values of some parameters are plotted in Figures (11-12).

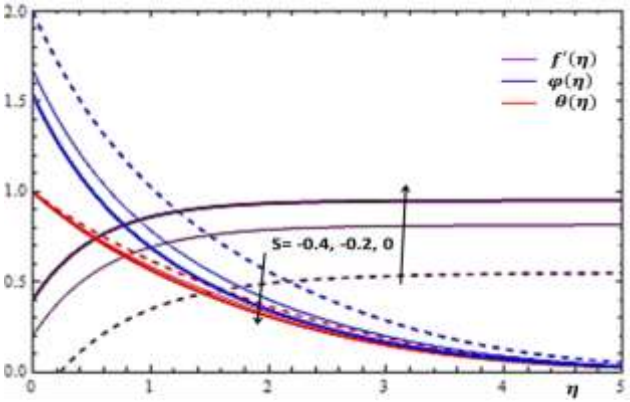

Figure 10. Effects of S on velocity, temperature and concentration profiles.

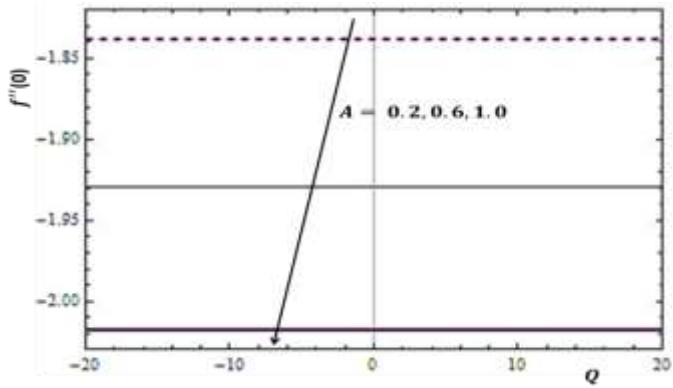

Figure 11. Variation of skin friction coefficient for different values of the unsteadiness parameter A along with the heat source parameter Q.

The results in Figure 11-12 indicate that the coefficient of skin friction is observed to decline as the values of the unsteadiness parameter Aincrease along with the increase in the heat source parameter Q or the chemical reaction parameter γ.

Both heat source/sink and chemical reaction parameters have no effect on skin friction coefficient. Further results on the variations of skin friction coefficient,

Nusselt number and Sherwood number with respect to some pertinent parameters is presented in Table 3.

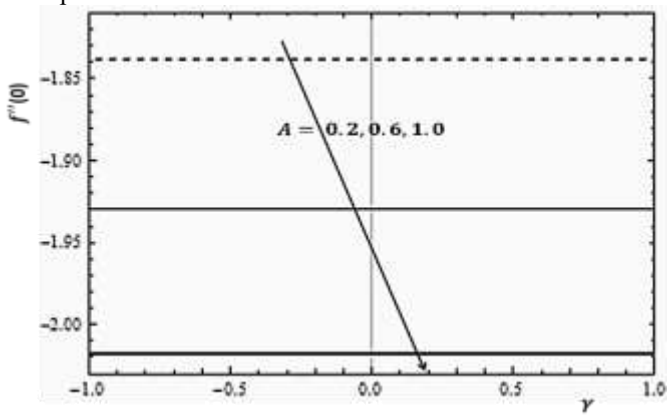

Figure 12. Variation of skin friction coefficient for different values of the unsteadiness parameter A along with the chemical reaction parameter γ.

Table 3. Coefficients of Skin-friction, Nusselt number and Sherwood number.

A	λ	M	R_d	S	S_c	Q	γ	$-f''(0)$	$-\theta'(0)$	$-\varphi'(0)$
0.1								1.58556	0.569631	1.43037
0.2								1.60972	0.637310	1.36269
0.3	0.1							1.63367	0.698930	1.30107
	0.2							1.62921	0.564361	1.43564
	0.3	1.0						1.71973	0.690822	1.30918
		2.0						2.01674	0.669738	1.33026
		3.0	0.1					2.27216	0.654251	1.34575
			0.2					2.27216	0.617937	1.38206
			0.3	0.2				2.27216	0.587700	1.41230
				0.3				2.27216	0.587700	1.41230
				0.4	1.0			2.38107	0.601453	1.39855
					2.0			2.50563	0.620985	1.37901
					3.0	0.1		2.50563	0.624377	1.37562
						0.2		2.50563	0.591982	1.40802
						0.3	0.1	1.81708	0.597492	1.40251
							0.2	1.81708	0.597492	1.40251
							0.3	1.81708	0.597492	1.40251

One can see from the table that the values of skin friction can be increased by increasing the unsteadiness parameter *A* or the magnetic parameter *M*. The local Nusselt number can be maximized by increasing the unsteadiness parameter *A* or Schmidt number *Sc*. It can also be enhanced by reducing the magnetic parameter *M* or the radiation parameter *Rd*. Also, the local Sherwood number

can be increased by increasing the magnetic parameter M or the radiation parameter Rd. It can also be increased by reducing the unsteadiness parameter A or Schmidt number Sc.

CONCLUSION

In this study, efforts were made to improve existing models by considering additional parameters such as the effects of heat source and chemical reaction in the flow models. On the other hand, a powerful method, namely the homotopy analysis method was used and the results agreed with previous reports. In conclusion, the impacts of pertinent parameters on velocity, temperature and nanoparticles volume fraction profiles are summarized as follows:

•The flow velocity can be accelerated by reducing the values of the unsteadiness, Maxwell viscoelastic, magnetic or permeability parameters;
•The temperature profile can be maximized in the boundary region by increasing the values of Maxwell, magnetic, permeability or heat source parameters. This profile can also be enhanced by reducing the effects of unsteadiness or radiation parameters;
•The concentration of nanoparticles can be raised by increasing the Maxwell, magnetic, permeability or chemical reaction parameters. The concentration profile can also be raised by minimizing the unsteadiness, radiation or heat source parameters. Moreover, the results obtained in the present study were also found to be in a nice agreement with previous works under some restricted assumptions.

REFERENCES

Awais, M., Hayat, T., Irum, S and Alsaedi, A. (2015). Heat generation/absorption effects in a boundary layer stretched flow of Maxwell nanofluid: analytic and numeric solutions. *PLoS One* **10**(6): DOI: 10.1371/journal.pone.0129814.

Chamkha, J., Aly, M and Mansour, A. (2010). Similarity solution for unsteady heat and mass transfer from a stretching surface embedded in a porous medium with suction/injection and chemical reaction effects. *Chemical Engineering Communications* **197**(6): 846-858. https://doi.org/10.1080/00986440903359087.

Choi, U.S and Eastman, J.A. (1995). Enhancing thermal conductivity of fluids with nanoparticles. *Proceedings of the ASME* **66**:99–105.

Elbashbeshy, E., Abdelgaber, K and Asker, H. (2018). Heat and mass transfer of a Maxwell nanofluid over a stretching surface with variable thickness embedded in porous medium. *International Journal of Mathematics and Computational Science* **4**(3): 86-98. http://www.aiscience.org/journal/ijmcs

Ijaz, M and Ayub, M. (2019). Nonlinear convective stratified flow of Maxwell nanofluid with activation energy. *Heliyon* **5**(1): 1-31. DOI: 10.1016/j.heliyon.2019. e01121

Liao, J. (2003). Beyond Perturbation: Introduction to Homotopy Analysis Method. Chapman and Hall/CRC, USA.

Mabood, F., Imtiaz, M., Alsaedi, A and Hayat T. (2016). Unsteady convective boundary layer flow of Maxwell fluid with nonlinear thermal radiation: A numerical study. *International Journal of Nonlinear Sciences and Numerical Simulation* **17**(5): 221–229. DOI: https://doi.org/10.1515/ijnsns-2015-0153.

Madhu, M., Kishan, N and Chamkha, J. (2017). Unsteady flow of a Maxwell nanofluid over a stretching surface in the presence of MHD and thermal radiation effects. *Propulsion and Power Research* **6**(1):31–40. http://dx.doi.org/10.1016/j.jppr. 2017. 01.002.

Mukhopadhyay, S., Ranjan, P and Layek, G.C. (2013). Heat transfer characteristics for the Maxwell fluid flow past an unsteady stretching permeable surface embedded in a porous medium with thermal radiation. *Journal of Applied Mechanics and Technical Physics* **54**(3): 385–396. DOI: 10.1134/S0021894413030061.

Mukhopadhyay, S and Bhattacharyya K. (2012). Unsteady flow of a Maxwell fluid over a stretching surface in presence of chemical reaction. *Journal of the Egyptian Mathematical Society* **20**, 229–234. DOI: 10.1515/ijnsns-2015-0153.

Nadeem, S., UlHaq, R and Khan, H. (2013). Numerical study of MHD boundary layer flow of a Maxwell fluid past a stretching sheet in the presence of nanoparticles. *Journal of the Taiwan Institute of Chemical Engineers* **45:**121-126. http://dx.doi.org/10.1016/j.jtice.2013.04.006.

Ramesh, G.K and Gireesha, B.J. (2014). Influence of heat source/sink on a Maxwell fluid over a stretching surface with convective boundary condition in the presence of nanoparticles. *Ain Shams Engineering Journal* **5**: 991–998. http://dx.doi.org/10.1016/j.asej.2014.04.003.

Sharidan, S., Mahmood, T and Pop, I. (2006). Similarity solutions for the unsteady boundary layer flow and heat transfer due to a stretching sheet. *International Journal of Applied Mechanics and Engineering* **11**(3): 647-654.

Sravanthi, C.S and Gorla, R.S. (2018). Effects of heat source/sink and chemical reaction on MHD Maxwell nanofluid flow over a convectively heated exponentially stretching sheet using homotopy analysis method. *International Journal of Applied Mechanics and Engineering* **23**(1):137-159. DOI: 10.1515/ijame-2018-0009.

Zhao, Y and Liao, S.J. (2013). Advances in the homotopy analysis method. World Scientific Publishing Co. Pte. Ltd., Singapore.